Millimeter wave generation for 6G applications using a semiconductor optical amplifier-based ring cavity laser system

SINDHU MUTHUDURAI[1, *], SIVANANTHARAJA AVANINATHAN[1], SELVENDRAN SAKKARAI[2], ESAKKI MUTHU KADARKARAI[3]
[1]*Department of Electronics and Communication Engineering, Alagappa Chettiar Government College of Engineering and Technology, Karaikudi, Tamil Nadu, India*
[2]*School of Electronics Engineering (SENSE), Vellore Institute of Technology, Chennai 600127, India*
[3]*Department of Electronics and Communication Engineering, Anna University Regional Campus, Madurai 625019, India*

The growing demand for high-frequency communication in 6G applications has led to significant interest in millimeter-wave (mm-wave) signal generation. To address many of the issues that electronic components confront, photonic methods that transfer signals into the optical domain for processing present a possible way forward. This paper explores the use of a Semiconductor Optical Amplifier-based Ring Cavity Laser System for the generation of mm-wave signals through optical signals. The proposed scheme eliminates the need for an external laser or pump source, thereby substantially reducing the system's complexity and cost. The transmission performance is evaluated by modulating 10 Gbps data and transmitting it over 50 km of optical fiber, that achieves a satisfactory Bit Error Rate (BER) and clear eye diagrams. Furthermore, this scheme can generate tunable mm-waves ranging from 1 GHz to several THz, with output power of around -15.4 dBm at 200 GHz.

(Received March 24, 2025; accepted October 10, 2025)

Keywords: Semiconductor Optical Amplifier (SOA), Millimeter-wave (mm-wave), Ring Cavity Laser System, 6G

1. Introduction

The relentless progression of mobile communication technologies is propelling the exploration of ultra-high-frequency spectra, driven by the insatiable demand for unprecedented data throughput and near-instantaneous latency envisioned for 6G-era applications. Millimeter-wave (mm-wave) frequencies, typically in the range of 30 GHz to 300 GHz, are viewed as a promising solution to meet these requirements [1, 2]. However, the use of mm-waves for mobile communications has been considered impractical due to their high propagation losses and susceptibility to signal blockage. These signals are easily obstructed not only by physical barriers such as buildings and vegetation but also by human bodies, making the deployment of mm-wave networks challenging, particularly in urban environments [3]. Despite these challenges, recent developments have led to increased interest in mm-wave technologies, as they offer vast bandwidths and high data transmission rates, essential for the expected data traffic growth in the coming decades [4]. To overcome the limitations posed by propagation losses and ensured reliable communication; it is crucial to integrate high-performance components that can compensate for these losses and enhance the overall network coverage. Semiconductor Optical Amplifiers (SOAs) have emerged as a promising solution to address these issues in mobile communication systems. SOAs offer several advantages, such as their ability to amplify signals effectively, thereby extending the reach of signals and improving network performance. Unlike traditional electronic amplifiers, SOAs operate optically, which significantly reduces the losses encountered in conventional wireless transmission and enables more efficient signal propagation over long distances. SOAs are characterized by several key features that make them particularly suitable for mm-wave generation in 6G applications. These include their substantial nonlinearities, which allow for efficient signal amplification and frequency conversion; low power consumption, which is essential for sustainable operation in next-generation networks; wavelength tunability, offering flexibility in system design; a wide dynamic range and rapid response, which enhance signal integrity and system responsiveness; and their compact size, allowing integration into small, cost-effective chips [5-8]. Additionally, the cost-effectiveness of SOAs, especially in comparison to other optical amplifiers like Erbium-Doped Fiber Amplifiers (EDFAs), makes them an attractive option for systems where minimizing complexity and cost is crucial. Unlike EDFAs, which require an external pump laser to operate, SOAs integrate all necessary components on a single chip, eliminating the need for additional, expensive pump sources. This inherent simplicity and cost-efficiency, combined with their robust performance in high-frequency ranges, position SOAs as an ideal candidate for use in the generation and amplification of signals for 6G communication networks. This paper explores the

potential of SOAs for mm-wave generation in the context of 6G communication systems. The role of SOAs in mitigating the challenges of signal attenuation in the ring cavity, enhancing network reach, and ensuring cost-effective integration into next-generation mobile networks is examined. By leveraging the unique properties of SOAs, this work aims to contribute to the development of scalable, efficient, and high-performance systems that will enable the deployment of reliable mm-wave communication networks for 6G applications.

2. SOA-based ring cavity laser system architecture

The schematic representations of the signal generation system, RoF system, and receiver block in the SOA-based Ring Cavity Laser System architecture are shown in Figs. 1(a), 1(b), and 1(c), respectively.

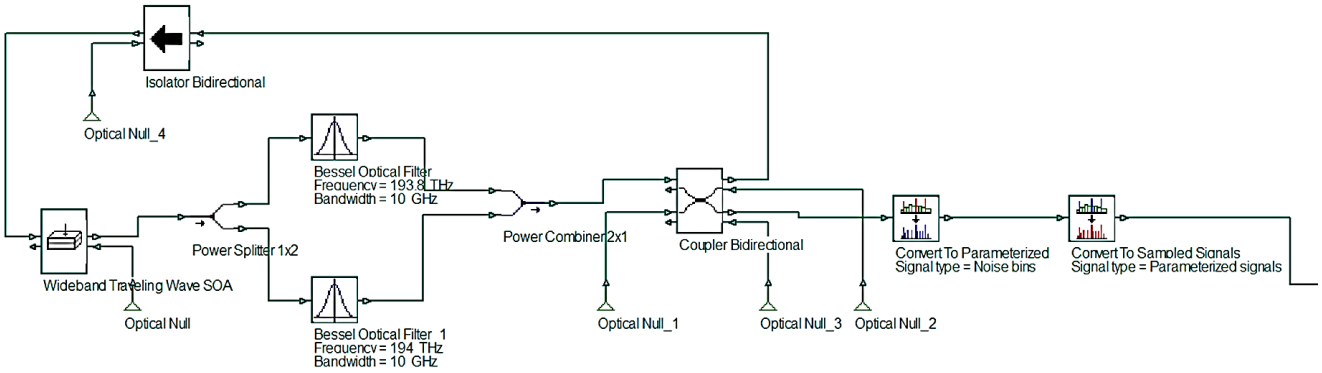

Fig. 1(a). Signal generation system (colour online)

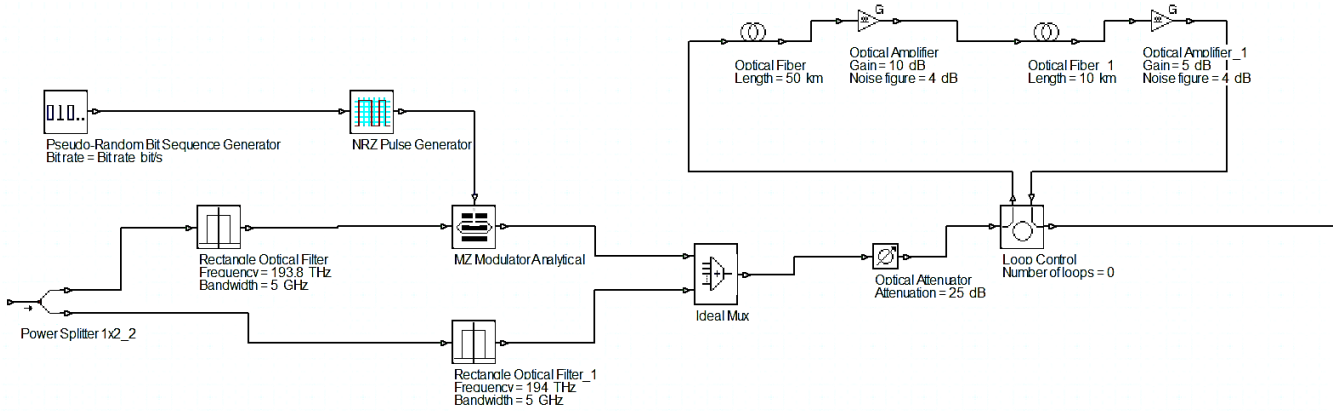

Fig. 1(b). RoF system (colour online)

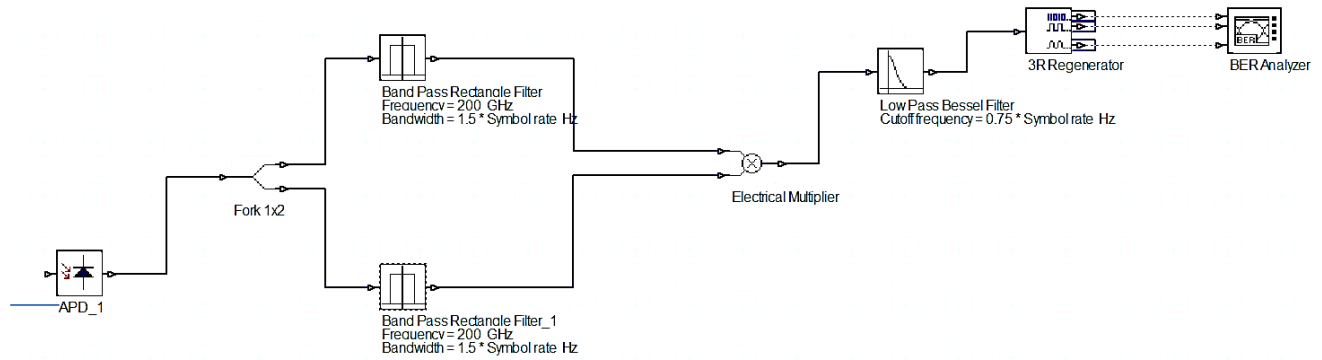

Fig. 1(c). Receiver block (colour online)

In this system, the SOA is optimized to deliver a strong optical output at 1550 nm. The intense output spectrum is split into a dual-frequency spectrum, centered at 193.8 THz and 194 THz, with a frequency separation of approximately 200 GHz which is the intended frequency. These frequencies are then combined and fed into the coupler. The output from the coupler is directed to convert noise bins to parameterized signal and subsequently converted into sampled signals for simulation purposes. The sampled output is then split into two signals using a rectangular optical filter with a bandwidth 5 GHz and the signal at 193.8 THz is modulated using a Mach-Zehnder Modulator (MZM). A Pseudo-Random Bit Sequence Generator, operating at a data rate of 10 Gb/s, generates a random bit sequence that is fed into a Non-Return-to-Zero (NRZ) pulse generator. The output of the NRZ pulse generator is then applied to the MZM to produce the optical modulated signal. This modulated signal, along with the signal at 194 THz, is sent into the multiplexer. The multiplexed signal is passed through an attenuator, which reduces the optical signal power by 25 dB before being transmitted through a 50 km optical fiber. This fiber is followed by a 10 km-long Dispersion Compensating Fiber (DCF), with optical amplifiers placed after each fiber to compensate for the span loss forming a closed loop. The dispersion parameter for a 50 km long SMF is 17 ps/nm-km [9]. As a result, the total accumulated dispersion is 17 × 50 = 850 ps/nm. This amount of dispersion can be compensated using a 10 km long DCF with a dispersion of -85 ps/km-nm, as illustrated in Fig. 2.

On the receiver side, the APD converts the optical signal into an electrical signal, which is then split into two equal parts and passed through Bandpass Rectangular Filters to extract the 200 GHz frequency signals. Both signals are then fed into the mixer, thereby eliminating the need for an RF Local Oscillator. The output of the mixer generally yields an intermediate frequency (IF) signal, resulting from the mixing process between the incoming signal and the local oscillator signal, which, in this case, is the extracted 200 GHz signal. The intermediate frequency can correspond to either the sum or the difference of the two frequencies involved in the mixing process. In this case, it is 400 GHz, as shown in Fig. 2(l). The output of the mixer is subsequently passed through a low-pass filter (LPF) to recover the transmitted data in the proposed system as shown Fig. 2(m). The values of the Q-factor, Log (BER), and received power are shown in Table 2.

3. Numerical analysis

For the ease of convenience, consider a basic sinusoidal data source that is applied to modulate the signal using a single-drive Mach Zehnder Modulator at the transmitter. At the receiver, the target millimeter-wave (mm-wave) carrier frequency is detected following the photodetector (PD). The electric fields corresponding to the two signals in the proposed scheme can be expressed as [10]:

$$A_1(t) = A_1 \exp j\,(2\pi f_1 t + \phi_1), \tag{1}$$

$$A_2(t) = A_2 \exp j\,(2\pi f_2 t + \phi_2), \tag{2}$$

Here A_1 and A_2 represent the peak amplitudes of the electric fields, while f_1 and f_2 denote the optical frequencies of the two signals. The desired mm-wave frequency f_{mmw} is given by the difference f_1- f_2. The phase noises of the two independent signals are represented by ϕ_1 and ϕ_2. For simplicity we assume that $A_1 = A_2 = 1$ and the modulating signal is sinusoidal, which can be expressed as $m(t) = m \cos(2\pi f_m t)$.

Fig. 1(b) illustrates the principle of the proposed scheme, where a single carrier is modulated, while the other signal is transmitted as an optical local oscillator (LO) in parallel with the modulated carrier. Accordingly, the electric fields of both the modulated and unmodulated optical carriers can be expressed as follows:

$$V_1(t) = \exp j\left[2\pi f_1 t + \frac{1}{2}(m \cos 2\pi f_m t + \theta) + \phi_1\right] \tag{3}$$

$$V_2(t) = \exp j\,(2\pi f_2 t + \phi_2). \tag{4}$$

In equation (3), m represents the modulation index of the single-drive Mach-Zehnder modulator (MZM), f_m denotes the frequency of the modulated millimeter-wave signal, and θ refers to the bias phase shift of the modulator.

The Bessel representation is expressed as:

$$V_1(t) = \sum_{n=-\infty}^{\infty} j^n J_n\left(\frac{m}{2}\right) \exp j\left(2\pi(f_1 + + nf_m)t + \frac{\theta}{2} + \phi_1\right) \tag{5}$$

$$V_2(t) = \exp j\,(2\pi f_2 t + \phi_2). \tag{6}$$

Here, $J_n\left(\frac{m}{2}\right)$ represents the Bessel function of the first kind of order n with the argument $\frac{m}{2}$ which is used to generate all orders of sidebands resulting from external modulation. The transfer function for the dispersive element of the single-mode fiber (SMF) is expressed as:

$$H(j\omega) = \exp\left(j\frac{1}{2}\beta_2 l\omega^2\right)$$

The system frequency response is denoted by ω, the fiber length by l, and the second-order fiber dispersion coefficient owing to chromatic dispersion by β_2.

After transmission through the single-mode fiber (SMF), Equations (5) and (6) are modified as follows:

$$V_{f1}(t) = \sum_{n=-\infty}^{\infty} j^n J_n(m) \exp j \left[2\pi(f_1 + nf_m)t + \frac{\theta}{2} + \phi_1\right] . \exp\left(j\frac{1}{2}\beta_2 l\omega^2\right)$$

$$V_{f2}(t) = \exp j\,(2\pi f_2 t + \phi_2). \exp\left(j\frac{1}{2}\beta_2 l\omega^2\right). \quad (7)$$

The analytical expression after the photodetector (PD) can be written as:

$$i_p(t) = \Re \text{ x } \sum_{n=-\infty}^{\infty}.\sum_{p=-\infty}^{\infty}. j^{n-p} J_n(m) J_p(m) \text{ x}$$

$$\text{x exp j } (n^2 - p^2)\,(0.5\beta_2 l\omega^2) \text{ x}$$

$$\text{x } \{\exp j\,[4\pi\,(n-p)f_m t + 2\theta] +$$

$$+ \{\exp j\,[2\pi\,(f_1 - f_2) + (n-p)f_m\}t + (\phi_1 - \phi_2) + \theta]\} + \exp j\,[2\pi\{(f_1 - f_2) +$$

$$+ (n-p)f_m\}t + (\phi_1 - \phi_2) + \theta] \quad (8)$$

Here, $\Re$ represents the responsivity of the photodetector (PD). The beating process occurs in the PD between the generated sidebands and optical carriers. The interaction between the two optical modes leads to the generation of the desired electrical signal at the millimeter-wave range, along with various orders of electrical harmonic components. The last three terms in Equation (8) clearly demonstrate the desired modulated millimeter-wave frequency at ($f_1 - f_2$) along with the corresponding uncorrelated phase noise ($\phi_1 - \phi_2$). Phase noise in SOAs can significantly impact optical communication systems, particularly those employing coherent detection. While SOAs effectively amplify signals, they introduce phase noise mainly due to amplified spontaneous emission (ASE), carrier density fluctuations, and nonlinear effects such as four-wave mixing (FWM).

ASE is inherently random in phase and when amplified, broadens the signal linewidth, leading to potential bit errors in coherent systems [12, 14, 16-20].

Carrier density fluctuations induce intensity noise, which changes the refractive index and leads to phase variations in the amplified signal [12, 14-16].

FWM, a nonlinear mixing process, can transfer phase noise from pump and signal waves to generated conjugate waves, affecting wavelength conversion performance [12].

These phase noise effects can distort signal constellations, increasing bit error rates [12, 13, 21-23]. Common mitigation methods include:

(i) Using SOAs with lower linewidth enhancement factors and optimizing bias currents and input powers [13, 24-26].

(ii) Employing modulation formats less sensitive to phase noise, such as DPSK [24, 27-29]; and Implementing phase noise cancellation techniques at the receiver [12, 13].

However, in the proposed architecture, the SOA operates without an external laser input. Instead, the system generates signals by amplifying ASE within a ring cavity, where the ASE undergoes constructive interference through controlled recirculation. As the signal generation process originates from ASE noise itself, traditional concerns regarding phase noise – which primarily relate to preserving the coherence and spectral purity of external laser inputs – are not directly applicable. Rather, the ring cavity design inherently manages phase noise by selectively enhancing specific longitudinal modes, resulting in stable millimeter-wave beat signals without requiring external phase noise suppression techniques such as injection locking or linewidth narrowing.

4. Experiment and results

The schematic for mm-wave generation is presented in Fig. 1. It is hypothesized that an optimized Semiconductor Optical Amplifier (SOA) can achieve peak gain, with the relevant parameters of the optimized SOA detailed in Table 1. The saturation power of the SOA is a critical factor in achieving peak gain, as it significantly influences both the linear and nonlinear characteristics of the amplifier. The saturation power is given by the equation (Connelly, 2002):

$$P_{sat} = \frac{A}{\Gamma} . I_s$$

where A represents the active region cross-sectional area, Γ denotes the optical confinement factor, and I_s is the saturation intensity, expressed as:

$$I_s = \frac{h\nu}{a_{N.}\,\tau}$$

Here, h is Planck's constant, a_N is the differential modal gain, v is the optical frequency, and τ is the spontaneous carrier lifetime. To enhance the saturation output power, it is essential to minimize the optical confinement factor Γ, as it is inversely proportional to the saturation power. The optimization of injection current is necessary since lower bias currents result in reduced gain and lower saturation output power [11]. The parameters of the SOA were optimized using the Multi-Parameter Optimization (MPO) tool in the Optisystem simulation environment, and the optimized values are summarized in Table 1. The confinement factor was set to 0.4. While higher confinement factors can increase modal gain, they also lead to higher carrier density depletion, resulting in faster gain recovery but potentially reduced saturation output power. A confinement factor of 0.4 provides a balance between modal gain and output power stability.

The bias (injection) current significantly influences carrier pumping rate and thus optical gain by increasing the electron density in the excited state. However, higher bias currents lead to increased power consumption and thermal effects [30]. Therefore, a bias current of 0.45 A was chosen to ensure sufficient gain while maintaining thermal stability and efficiency. The active region length was set at 600 μm. Increasing the length enhances optical gain due to the longer interaction path between carriers and photons, but excessive length can introduce amplified spontaneous emission (ASE) noise and increase device footprint. A length of 600 μm was thus selected as an optimal compromise. These SOA parameters are feasible for real-world fabrication using established semiconductor manufacturing techniques such as Molecular Beam Epitaxy (MBE) and sub-micron photolithography, enabling precise control over layer composition and thickness [31-33]. Other parameters were retained at their nominal values to isolate and analyse the impact of these critical design variables on system performance. This comprehensive parameter optimisation ensures that the SOA design is practical, efficient, and well-suited for the proposed application.

The adjustments resulted in highly intensified amplified pulses as shown in Fig. 2(a). Then the desired mm-wave can be generated by optical heterodyning. When two optical signals with central frequencies ω_1 and ω_2 (in this case, ω_1=194 THz and ω_2=193.8 THz) are transmitted through an optical system and then mixed or "beat" at a photodetector, the result will be a difference frequency signal that lies in the millimeter-wave (mm-wave) range as demonstrated by the Equation (8).

The output of the Avalanche Photodiode (APD), as shown in Fig. 2(k), contains a clear difference frequency signal within the millimeter-wave (mm-wave) range at 200 GHz, resulting from optical heterodyning between two optical carriers at 194 THz and 193.8 THz. This confirms successful generation of the intended mm-wave beat signal. The detected mm-wave signal was then split into two paths and fed into a mixer for frequency down-conversion. The mixer output, shown in Fig. 2(m), was passed through a low-pass filter (LPF) to remove higher-order frequency components and noise. The resulting time-domain waveform exhibits a well-defined periodic structure, indicating that the signal's integrity is preserved during down-conversion.

Table 1. Optimized SOA parameter

Parameter	**Values**
Injection current	0.45A
Input facet reflectivity	5e-5
Output facet reflectivity	5e-5
Active length	0.0006 m
Width	0.4e-6 m
Height	0.4e-6 m
Optical confinement factor	0.4
Recombination coefficient	360e+006 1/s
Group velocity	75e+006 m/s
Temperature	300 K

Table 2. Log (BER), Q-factor and received power of the SOA-based ring cavity laser system

Parameter	**Values**
Log (BER)	-56.057
Q-factor	15.81
Received Power (dBm)	-15.4

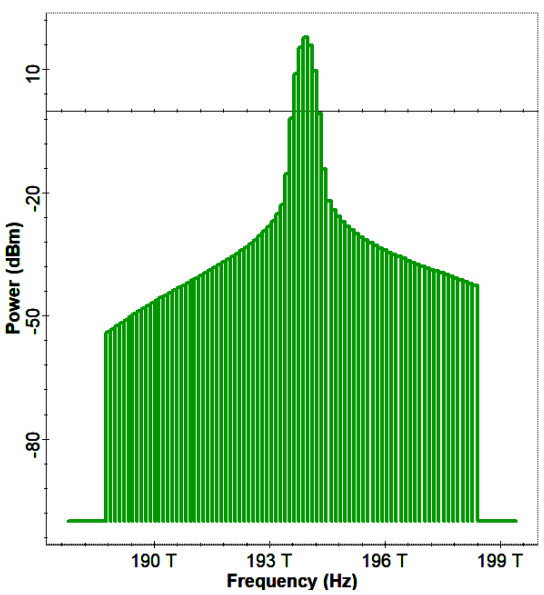
Power (dBm)
10
-20
-50
-80
190 T
193 T
196 T
199 T
Frequency (Hz)

(a)

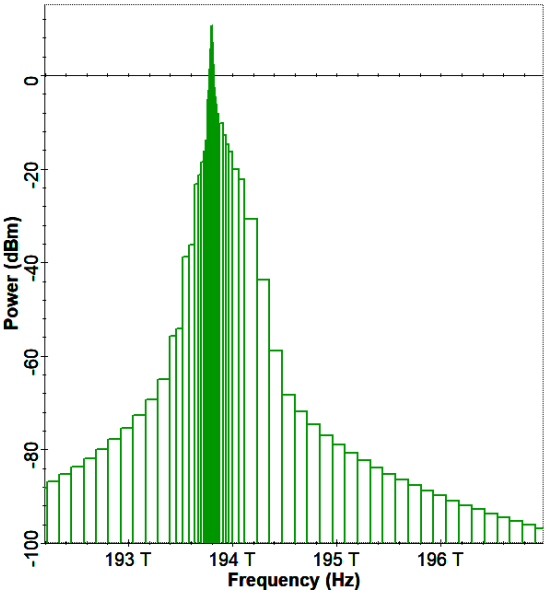
Power (dBm)
0
-20
-40
-60
-80
-100
193 T
194 T
195 T
196 T
Frequency (Hz)

(b)

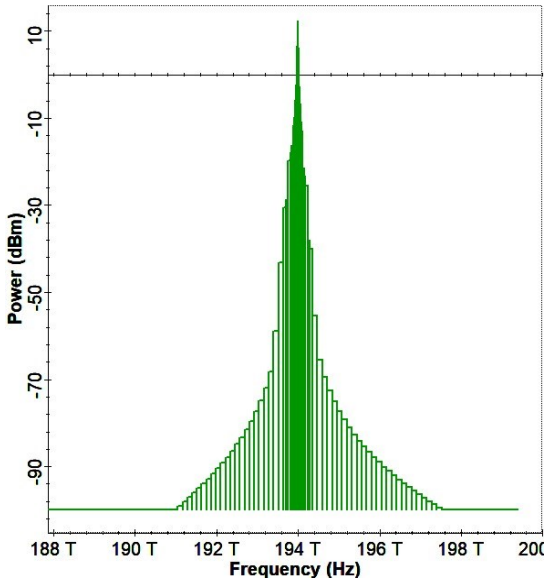
Power (dBm)
10
-10
-30
-50
-70
-90
188 T
190 T
192 T
194 T
196 T
198 T
Frequency (Hz)

(c)

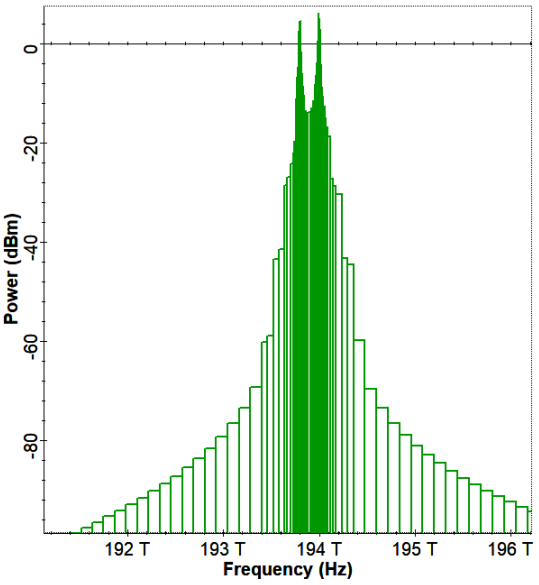
Power (dBm)
0
-20
-40
-60
-80
192 T
193 T
194 T
195 T
196 T
Frequency (Hz)

(d)

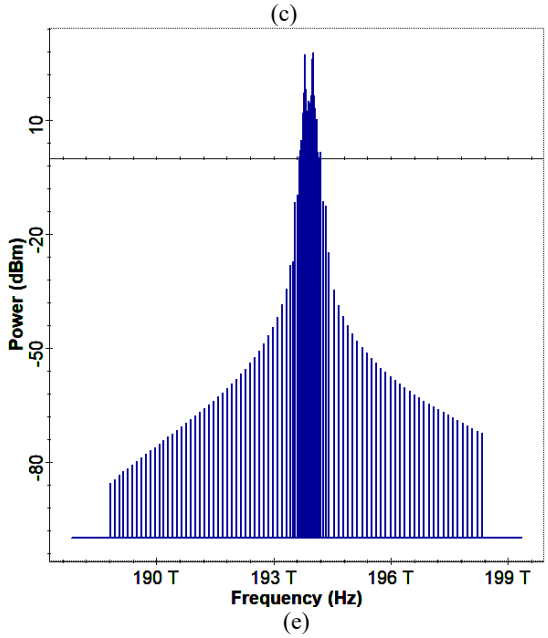
Power (dBm)
10
-20
-50
-80
190 T
193 T
196 T
199 T
Frequency (Hz)

(e)

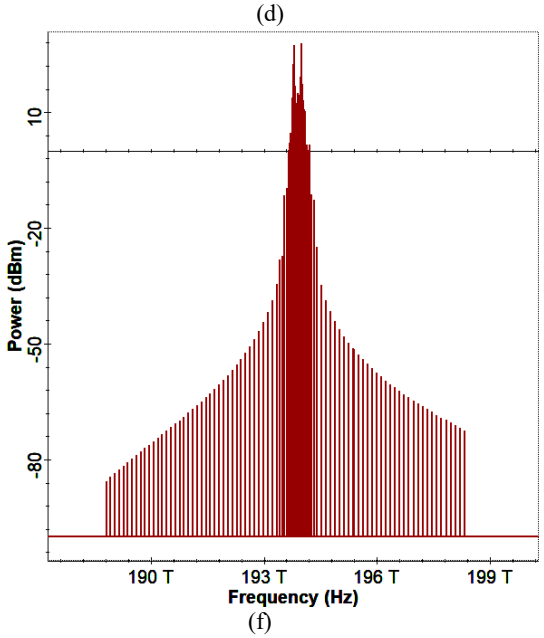
Power (dBm)
10
-20
-50
-80
190 T
193 T
196 T
199 T
Frequency (Hz)

(f)

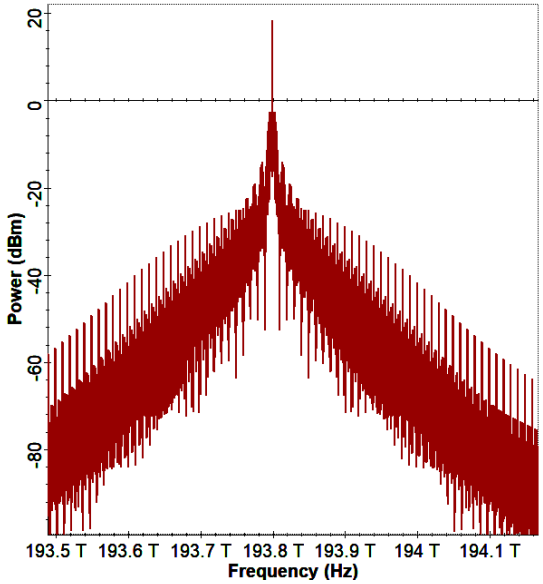
Power (dBm)
20
0
-20
-40
-60
-80
193.5 T
193.6 T
193.7 T
193.8 T
193.9 T
194 T
194.1 T
Frequency (Hz)

(g)

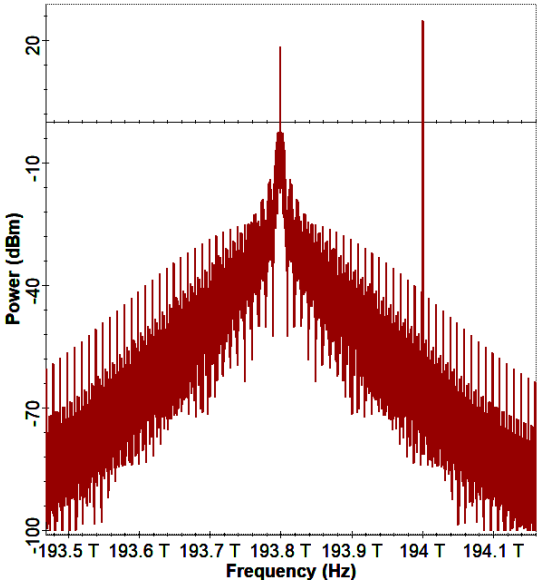
Power (dBm)
20
-10
-40
-70
-100
193.5 T
193.6 T
193.7 T
193.8 T
193.9 T
194 T
194.1 T
Frequency (Hz)

(h)

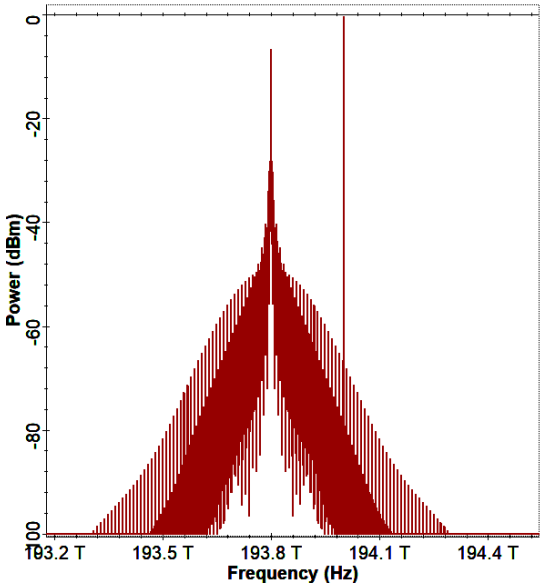
Power (dBm)
0
-20
-40
-60
-80
-100
193.2 T
193.5 T
193.8 T
194.1 T
194.4 T
Frequency (Hz)

(i)

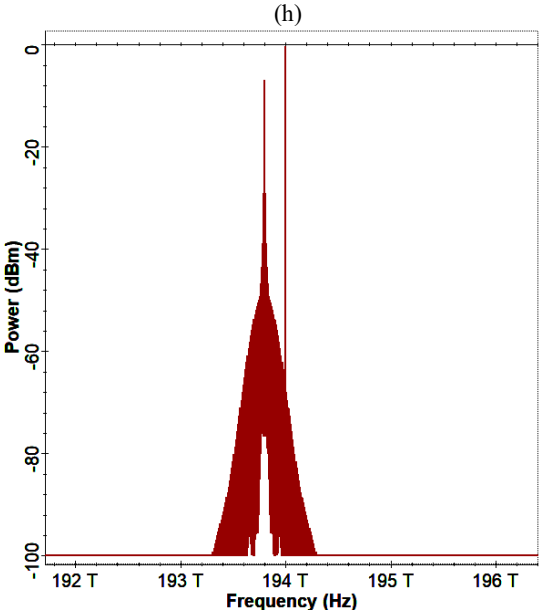
Power (dBm)
0
-20
-40
-60
-80
-100
192 T
193 T
194 T
195 T
196 T
Frequency (Hz)

(j)

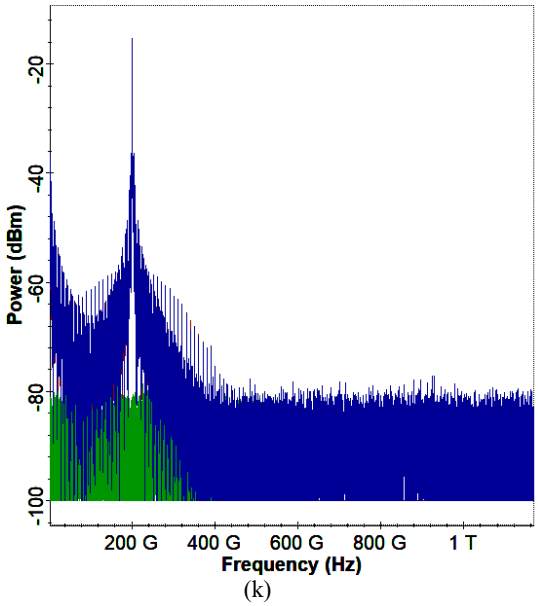
Power (dBm)
-20
-40
-60
-80
-100
200 G
400 G
600 G
800 G
1 T
Frequency (Hz)

(k)

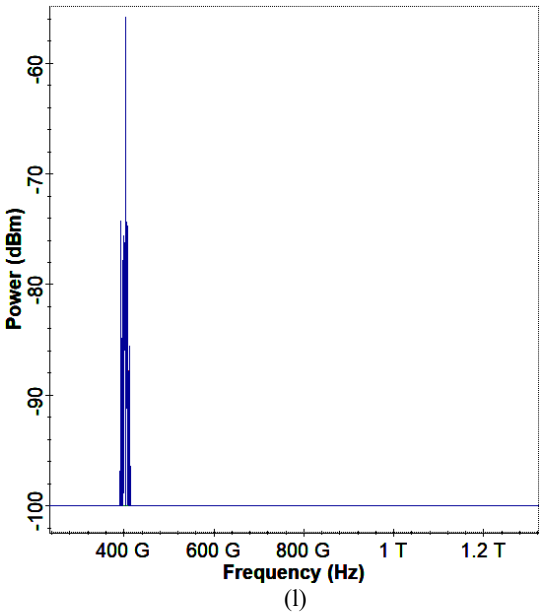
Power (dBm)
-60
-70
-80
-90
-100
400 G
600 G
800 G
1 T
1.2 T
Frequency (Hz)

(l)

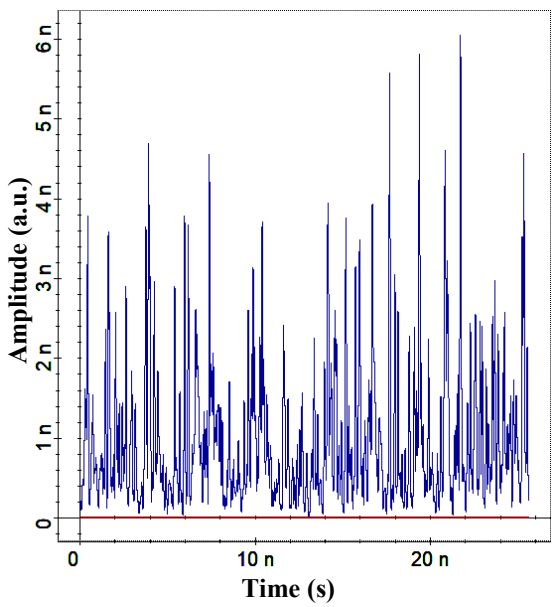

(m)

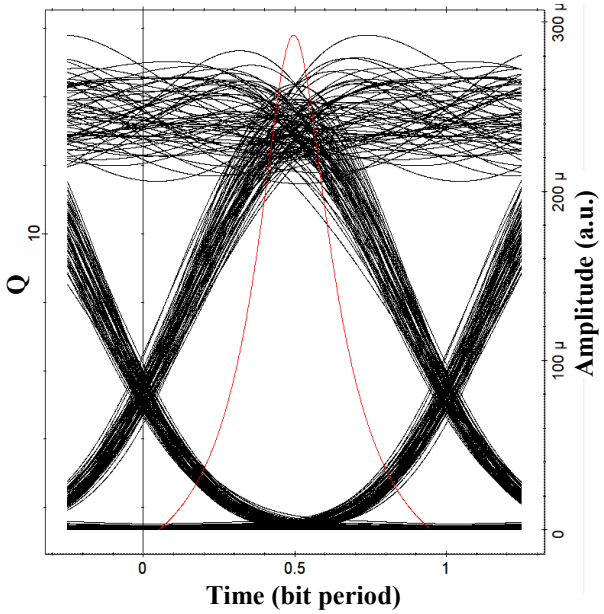

(n)

Fig. 2. Output spectrum (a) after SOA (b) after Bessel Filter (193.8 THz) (c) after Bessel Filter (194 THz) (d) after Coupler (e) after Convert to Parameterized (f) after Convert to Sampled Signals (g) after MZM (h) after MUX (i) after Attenuator (j) after Transmission loop (k) after APD (l) after Mixer (m) Low Pass Filter (LPF) (n) BER Analyzer (colour online)

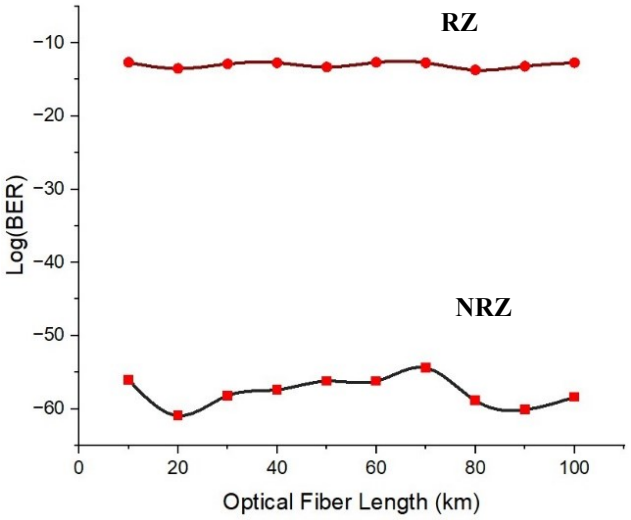

Fig. 3. Comparison of RZ and NRZ schemes (colour online)

To assess data modulation performance, both Non-Return-to-Zero (NRZ) and Return-to-Zero (RZ) formats were simulated. As shown in Fig. 3, NRZ modulation achieved a lower Bit Error Rate (BER) compared to RZ. This performance improvement is attributed to NRZ's higher spectral efficiency and better signal-to-noise ratio (SNR), making it more robust against distortions and noise during optical-to-electrical conversion.

Overall, these results demonstrate that the proposed system effectively generates high-frequency mm-wave signals with preserved data fidelity, especially under NRZ modulation, validating its suitability for high-speed wireless communication applications.

5. Conclusion

This paper investigates the use of a Semiconductor Optical Amplifier-based Ring Cavity Laser System for generating millimeter-wave signals in 6G communication applications. The novelty of the proposed scheme is that it eliminates the need for an external laser or pump source, reducing both complexity and cost. Experimental results show successful 10 Gbps data transmission over 50 km of Optical fiber with satisfactory Bit Error Rate (BER) and clear eye diagrams. The system also enables tunable mm-wave generation from 1 GHz to several THz, with an output power of around -15.4 dBm at 200 GHz. These results highlight the proposed scheme as a promising solution for efficient and cost-effective mm-wave signal generation in future high-frequency communication systems.

References

[1] Wei Hong, Zhi Hao Jiang, Chao Yu, Debin Hou, Haiming Wang, Chong Guo, Yun Hu, Le Kuai, Yingrui Yu, Zhengbo Jiang, Zhe Chen, Jixin Chen, Zhiqiang Yu, Jianfeng Zhai, Nianzu Zhang, Ling Tian, Fan Wu, Guangqi Yang, Zhang-Cheng Hao, Jian Yi Zhou, IEEE Journal of Microwaves **1**(1), 101 (2021).

[2] A. Tikhomorov, E. Omelyanchuk, A. Semenova,

Systems and Signals Generating and Processing in the Field of on-Board Communications, pp.1-5 (2018).
[3] G. R. MacCartney, T. S. Rappaport, S. Rangan, Proc. IEEE Global Commun. Conf. (GLOBECOM), pp. 1–7 (2017).
[4] Theodore S. Rappaport, Shu Sun, Rimma Mayzus, Hang Zhao, Yaniv Azar, Kevin Wang, George N. Wong, Jocelyn K. Schulz, Mathew Samimi, Felix Gutierrez, IEEE Access **1**, 335 (2013).
[5] Aneesh Sobhana, Aravind Anthur, Sean O'Duill, Mark Pelusi, Shu Namiki, Liam Barry, Deepa Venkitesh, Govind P. Agrawal, Advances in Optics and Photonics **14**(3), 571 (2022).
[6] Q. Wang, F. Zeng, H. Rideout, J. Yao, 2006 International Topical Meeting on Microwave Photonics, pp. 1-4 (2006).
[7] Tianliang Wang, Minghua Chen, Hongwei Chen, Jian Zhang, Shizhong Xie, IEEE Photonics Technology Letters **19**(16), 1191 (2007).
[8] Arwa Hassan Beshr, Moustafa H. Aly, Optical and Quantum Electronics **55**, 506 (2023).
[9] H. U. Bo-ning, Wang Jing, Wang Wei, Rui-mei Zhao, 2010 2nd International Conference on Industrial and Information Systems, doi: 10.1109/INDUSIS.2010.5565685 (2010).
[10] Drissa Kamissokoa, Jing Hea, Hassana Ganameb, Macki Talla, Optics Communications **474**, 126174 (2020).
[11] Paul Urquhart, Ed., Advances in Optical Amplifiers, Intech Open, 2011.
[12] A. P. Anthur, D. Venkitesh, R. Watts, J. O'Carroll, L. P. Barry, National Conference on Communications (NCC), pp. 1-5 (2013).
[13] M. Al-Qadi, M. O'Sullivan, C. Xie, R. Hui, IEEE Photonics Technology Letters **32**(7), 430 (2020).
[14] Wei Hong, Dexiu Huang, Xinliang Zhang, Guangxi Zhu, Optics Communications **281**(1), 28 (2007).
[15] Michael Connelly, C. L. Janer, Optical and Quantum Electronics **44**(3-5), 95 (2011).
[16] Emiel Dieussaert, Yanlu Li, Geert Morthier, Roel Baets, J. Phys.: Conf. Ser. **2041**, 012005 (2021).
[17] X. Li, F. Ruan, Y. Tang, T. Gao, S. Huang, Photonics **12**, 516 (2025).
[18] Sachinthani Alahakoon, Dushani Munasinghe, Gresha S. Samarakkody, Ruwan Weerasuriya, J. Phys. Commun. **4**, 09500 (2020).
[19] M. Pelusi, T. Kurosu, S. Namiki, Journal of Lightwave Technology **41**(5), 1375 (2023).
[20] Xinning Huang, Xiaoping Xie, Jiazheng Song,Tao Duan, Hui Hu, Xin Xu, Yulong Su, IEEE Journal **10**(4), 1 (2018).
[21] Mohammad Shahriar Khan Hemel, Md. Rownak Hossain, Mohammad Arif Sobhan Bhuiyan, Tan Jian Ding, Khairun Nisa Minhad, Kelvin Jian Aun Ooi, Sawal Hamid Md. Ali, Mamun Bin Ibne Reaz, Alexandria Engineering Journal **67**, 301 (2023).
[22] Anton Patyuchenko, Analog Dialogue **55**, 2 (2021).
[23] E. Rochat, R. Dandliker, IEEE Journal of Selected Topics in Quantum Electronics **7**(1), 49 (2001).
[24] Wei Hong, Dexiu Huang, Xinliang Zhang, Proceedings of SPIE **6782**, 67822L (2007).
[25] Babak Soltanian, Peter Kinget, IEEE Journal of Solid-State Circuits **41**, 1792 (2006).
[26] Ö. E. Aşırım, R. Huber, C. Jirauschek, Appl. Phys. B **128**, article number 218 (2022).
[27] G. P. Agrawal, Nonlinear Effects in Optical Fibers, Encyclopedia of Materials: Science and Technology (Second Edition), pp. 6218-6226 (2001).
[28] Jing Zhou, Duandan Liang, Photonics **8**(10), 428 (2021).
[29] Sukhbir Singh, Surinder Singh, Quang Minh Ngo, Amin Malek Mohammadi, Optical Fiber Technology **59**, 102323 (2020).
[30] R. Sarojini, A. Sivanantha Raja, S. Selvendran, K. Esakki Muthu, Optik - International Journal for Light and Electron Optics **185**, 852 (2019).
[31] Niloy K. Dutta, Qiang Wang, Semiconductor Optical Amplifiers, 2nd ed., Singapore: World Scientific, 85–115(2013).
[32] David J. Feng, C. L. Chiu, E. Y. Lin, T. S. Lay, T. Y. Chang, J. Appl. Phys. **45**, 2426 (2006).
[33] Thorlabs; https://www.thorlabs.com/newgrouppage9.cfm?objectgroup_id=7101&tabname=Wafer%20Fabrication#ad-image-0

*Corresponding author: sindhu.m15@outlook.com